Northumbria Research Link

Northumbria University
NEWCASTLE

University Library

Acousto-Pi: An Opto-Acoustofluidic System Using Surface Acoustic Waves Controlled With Open-Source Electronics for Integrated In-Field Diagnostics

Jethro Vernon[ID], Pep Canyelles-Pericas[ID], *Member, IEEE*, Hamdi Torun[ID], Xuewu Dai[ID],
Wai Pang Ng[ID], *Senior Member, IEEE*, Richard Binns[ID], Krishna Busawon[ID], *Senior Member, IEEE*,
and Yong-Qing Fu[ID]

Abstract—**Surface acoustic wave (SAW) devices are increasingly applied in life sciences, biology, and point-of-care applications due to their combined acoustofluidic sensing and actuating properties. Despite the advances in this field, there remain significant gaps in interfacing hardware and control strategies to facilitate system integration with high performance and low cost. In this work, we present a versatile and digitally controlled acoustofluidic platform by demonstrating key functions for biological assays such as droplet transportation and mixing using a closed-loop feedback control with image recognition. Moreover, we integrate optical detection by demonstrating *in situ* fluorescence sensing capabilities with a standard camera and digital filters, bypassing the need for expensive and complex optical setups. The Acousto-Pi setup is based on open-source Raspberry Pi hardware and 3-D printed housing, and the SAW devices are fabricated with piezoelectric thin films on a metallic substrate. The platform enables the control of droplet position and speed for sample processing (mixing and dilution of samples), as well as the control of temperature based on acousto-heating, offering embedded processing capability. It can be operated remotely while recording the measurements in cloud databases toward integrated in-field diagnostic applications such as disease outbreak control, mass healthcare screening, and food safety.**

Index Terms—**Feedback control, fluorescence imagining, integrated acoustofluidics, open-source electronics, piezoelectric thin film, point-of-care (POC) diagnostics, surface acoustic waves (SAWs).**

I. Introduction

IN ORDER to manage disease outbreaks and reduce its rapid spreading, fast, accurate, and affordable diagnostics techniques are needed. The most established techniques for medical diagnostics based on nucleic acid (DNA and RNA) detection are polymerase chain reaction (PCR) and loop-mediated isothermal amplification (LAMP) [1]. Both PCR and LAMP facilitate biological reactions that result in exponential amplification of targeted DNA for a subsequent detection step [2]. In these methods, the biological sample from the test subject is processed with a series of reagents in regulated protocols for DNA extraction, amplification, and detection, which require microfluidic functions such as mixing, dispensing, and heating. For DNA detection, the reagents produce a bound marker that is typically fluorescent to be optically measured in real-time during the amplification reaction. The luminescence level results in a positive or negative detection which is based on a predetermined threshold value. PCR is widely accepted as the gold standard diagnostic method of detection of viral DNA/RNA, including COVID-19 [3], whereas LAMP is emerging as an alternative technique that offers comparable performance [4]. PCR requires thermal cycling processes between 60 °C and 90 °C for around 40 cycles [5], [6], while LAMP is an isothermal process, commonly involving a constant temperature of 65 °C in the region of 20–30 min [6]–[8].

Surface acoustic wave (SAW) technology has found a wide range of applications including radio frequency (RF) filters in telecommunications, sensing, acoustofluidics, lab-on-a-chip (LOC), and biomedicine applications [9]–[13]. SAW technology has been used to realize PCR and LAMP functions for the detection of malaria [14], sexually transmitted pathogens [15], and salmonella [16]–[19]. SAWs are generated by applying RF signals to the interdigitated transducers (IDTs) patterned on the substrate of a piezoelectric material. SAW energy can be transferred into a liquid in contact with the device's surface to generate different functions for bio-sampling and biosensing [20], [21]. These functions are versatile and allow integrated LOC devices developed for diagnostic assays, tissue engineering, or drug development and delivery applications [22]–[24].

Different acoustofluidic functions in microfluidics, including generation, pumping, splitting, jetting, mixing, and heating of droplets, have been realized [25]. However, their integration into a single, low-cost, and efficient platform provided with a simple and low-cost optical detection for biological assays remains a challenge that this work aims to fulfill. This causes practical implications when using PCR to detect and model the spread of a disease outbreak. In current PCR tests, the sample is typically collected in one location, sent (refrigerated) to another, and the test result is usually given 24 h after the sample is collected. The setup presented here can be used in the field directly, and the test result can be automatically transmitted to a safe database to study virus transmission and infection rates, attributed to the embedded electronics. Another key aspect is that low-cost PCR machines consist only of thermal cyclers, with the detection being made in an endpoint mode using electrophoresis. This requires a skilled operator to run the detection test and interpret the result, which is time-consuming and difficult to integrate.

Opto-acoustofluidics is an emerging field that combines acoustics, fluid dynamics, and optics. Their combination can be done in several ways depending on the target application and optical-sensing technique applied, including but not limited to the photoacoustic effect. For instance, the latter can be used to detect low concentrations of cells inside a droplet, although requiring laser excitation source and optical beam hardware [26], or using laser sources in combination with optical galvanometers for spatial micrometer resolution [27]. In comparison, the system presented here uses fluorescence-based detection with the off-the-shelve digital cameras and no additional light excitation and related optical hardware. In addition, advanced microscopy setups are currently being developed using open-source (Raspberry Pi) platforms [28]–[32]. Thus, we envision future applications that will combine such setups with the Acousto-Pi platform.

In this work, we present an opto-acoustofluidic system concept with potential for integration using Raspberry Pi as an embedded control unit. The focus of this work has been to demonstrate the suitability of the Raspberry Pi platform to perform closed loop control using digital and thermal cameras in combination with optical fluorescence detection. The results presented here have been employed using two benchtop instruments: a signal generator and an RF amplifier. However, throughout the article, we present alternative components for setup integration.

A. Background

Acoustofluidic research applications are starting to be implemented with open-source platforms. For instance, Ultraino [33] is a phased-array system using ultrasound to suspend samples in a 3-D space with applications in holography and 3-D particle manipulation. This uses an Arduino Mega with a driver board that connects several ultrasonic transducers. The system is controlled via a computer that runs calculations to map the ultrasonic field, highlighting pressure nodes and then manipulating them to control the position of a sample.

In another electronic interfacing system [19], mobile phones are used to generate and amplify signals using Bluetooth-connected speakers connected to a piezoelectric transducer (PZT) (e.g., PZT). These acoustic waves are used to induce acoustic streaming in a polydimethylsiloxane (PDMS) chamber. Images are then gathered using the mobile phone in a microscope setup [19].

Another open-source acoustofluidic system [34] has developed a low-cost multifunction system. This system works with audible frequency range devices controlled with Arduino microcontrollers and it is able to manipulate fluids flowing in microchannels while rotating particles. Multiple platforms have targeted portability as a key part into integrating these devices for real-world situations. For instance, handheld acoustofluidics [35] to combat hurdles such as removing the need for benchtop lab equipment, miniaturizing, and running the platform with battery power but capable of mixing liquids, nebulization, and particle alignment. One system in particular uses a Raspberry Pi to interface ultrasonic transducers [36] that are used to position small-scale objects on water or free moving on a surface, however, the feedback processing is made on a separate laptop running MATLAB software.

We have chosen Raspberry Pi as a platform for several reasons: compromise between performance and cost; ease of use and availability of Python libraries; possibility to interface and control hardware with the general-purpose input–output (GPIO) pins; the desktop operating environment (similar to a PC); remote access; embedded signal processing; data storage and transmission to the cloud; and access to a dedicated family of hardware that is periodically upgraded.

Arduino, Raspberry Pi, and other small microcontroller/PC-based systems will become the next stage in progressing toward acoustofluidic application and, especially, LOC and point-of-care (POC). Among these systems, our platform uses Raspberry Pi hardware integrally for interfacing, control, and data analysis to control samples on a surface of a SAW device and integrating optical sensing with a standard digital camera. In addition, we use the platform with industrially scalable thin-film SAW devices operated in the megahertz domain.

Raspberry Pi is also emerging as an alternative for microscopy and fluorescent imaging [29], [37], [30] that can combine optical and thermal control circuits to image microscopic Caenorhabditis cells [29]. For instance, a low-cost imaging system for teaching, research, and bioengineering is produced using a Raspberry Pi camera, commercial light-emitting diodes (LEDs), and acrylic filters combined with Python modules for data analyses to effectively investigate fluorescent images [37]. We use Raspberry Pi and 3-D printed structures with LED diffusion, optical filters, and focus adjustment. Using hue saturation and value (HSV) color model, the selected color of the fluorescence is found with upper and lower bounds for hue (color) and saturation (level of gray). The rest of the color spectrum is digitally filtered from the image using a mask leaving only the fluorescent droplet in the image to be measured based on brightness/intensity.
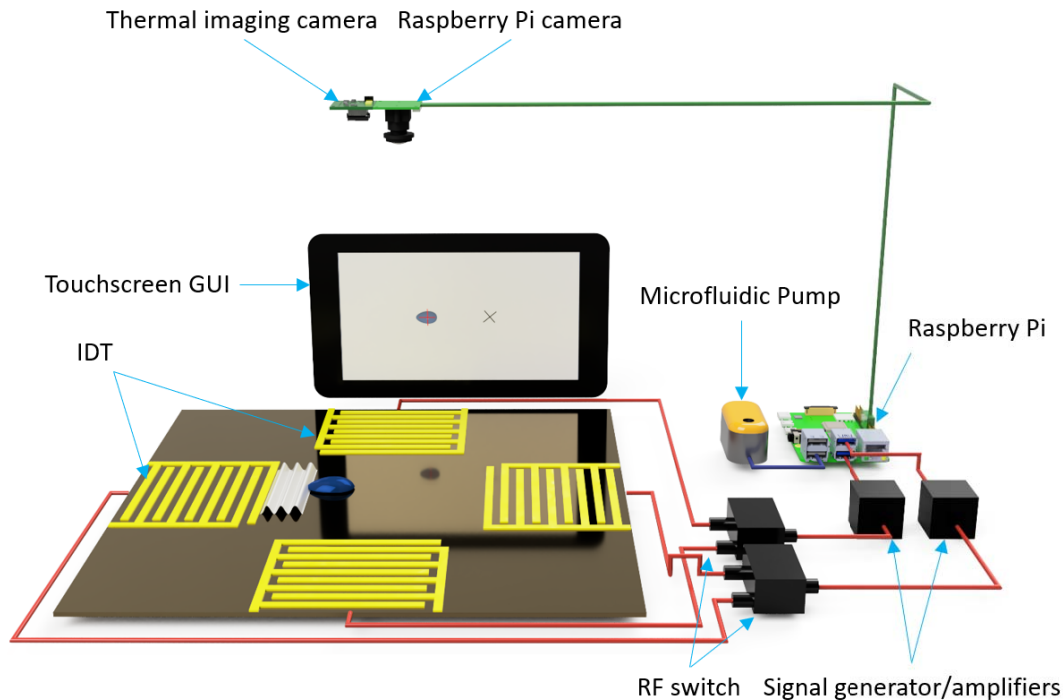
Fig. 1.   Illustration of SAW platform integrated with a Raspberry Pi controlling signal generators, amplifiers, RF switches, visible, and thermal cameras interfaced through a touchscreen.

B. Acousto-Pi Overview

Open-source electronics and additive manufacturing are now being used to produce high-quality scientific equipment for a low cost [38]. For instance, expensive syringe pumps have been realized with 3-D printing and open-source libraries, lowering the cost to below £100 [39]. The microfluidic protocol to extract and amplify DNA requires different volumes of components such as enzymes, primers, buffers, or fluorescent dyes. Microfluidic pumps could be employed to administer the microfluidic protocol necessary to run the biological reactions, facilitating further integration and automation. Similarly, in this work, we fill the gap in interfacing ultrasonic and optical hardware and control strategies with open-source means. Hence, we combine multiple SAW functions, closed-loop control systems, and camera-based fluorescent detection into a single acoustofluidic platform.

The platform is integrated with two cameras, for example, a Raspberry Pi camera and an infrared camera, which can be monitored simultaneously. The visible light camera is used for droplet position control and fluorescent measurements. The infrared camera is used for contactless temperature measurements (see Fig. 1). Taking advantage of Raspberry Pi and Python programming language, with low-cost but industrially scalable in-line processing, the system is able to be adaptive and interface with a large range of components and equipment needed for SAW and biological sample testing.

A computer vision library is used for droplet tracking and fluorescence measurements. Finally, Raspberry Pi has been embedded to control signal generators, microfluidic pumps, and thermal imaging cameras to create a multifunctional platform to perform and develop biological assays (Fig. 1). We have not included a network analyzer in Fig. 1 as the resonant frequencies of the SAW devices have been characterized beforehand. Plans are to provide network analyzer hardware capabilities using, for instance, a phase locked loop algorithm (as described in [35]). We envision that this platform could be employed in the POC systems for emergency situations such as the current COVID-19 pandemic, allowing for mass automated testing linked directly to government cloud databases such as test and trace [40]. In future versions, we will consider using the industrial version of Raspberry Pi (Zero) due to its compact design, scale up possibilities, and compatibility to Raspberry Pi hardware used.

II. DESIGN METHODOLOGY AND PROCEDURES

A. Hardware

We have developed an electronic testbed to automate the experimental procedures and data analysis. The embedded controller is based on a Raspberry Pi (model 4) due to its relatively low cost, versatility, and open-source nature. This offers an operating system comparable to a desktop PC, complemented with a dedicated hardware family that we make use, and with GPIO connections to interface electronic sensors and actuators. A Raspberry Pi camera (module V2), camera serial interface (CSI) port, and a touchscreen display (Official Raspberry Pi 7") are used with a display serial interface (DSI) port [41]. The thermal camera (Flir Lepton Series model 2.5) is connected to the Raspberry Pi using I-squared-C (I^2C) serial connection for temperature control and measurement. These cameras are used as main monitoring and control inputs for GUI.

For droplet transport, the SAW devices are excited using sine wave signals from a signal generator (Tektronix AFG1062) and amplifiers (Mini-Circuits ZHL-20W-13+).
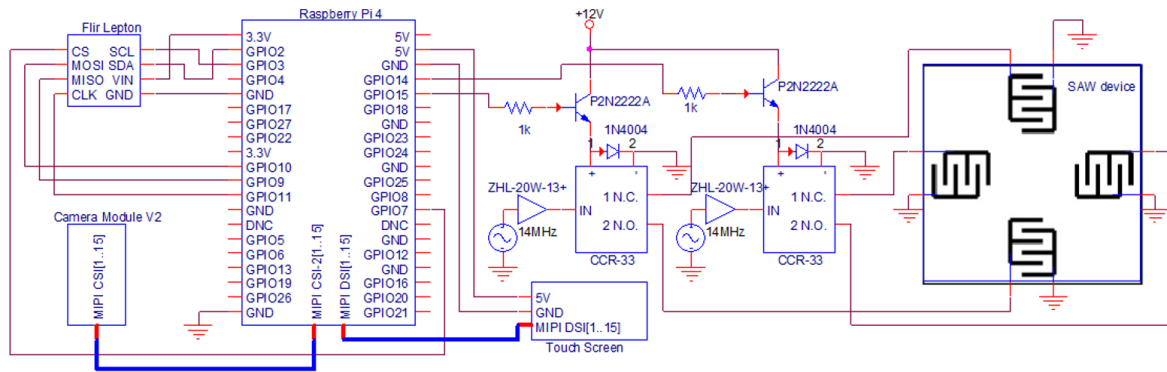
Fig. 2.   Circuit diagram of Raspberry Pi pinout and SAW control using an RF switch.
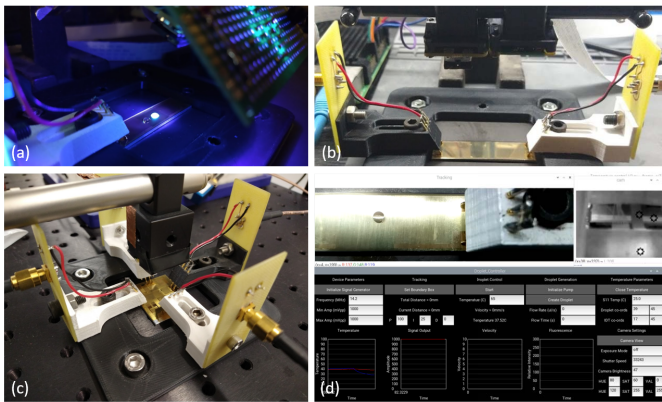

Fig. 3.   (a) Fluorescent droplet on SAW device. (b) Single-axis two IDT SAW device and 3-D mounted cameras. (c) Two-axis four IDT mounted SAW device. (d) GUI as seen on screen in the overall setup.

To control the different SAW devices on the platform (Fig. 1), powered RF switches (Teledyne CCR-33S1O) are used to switch between four IDTs on two axes (Fig. 2). The SAW signals are generated using a virtual serial com port over USB, and Python scripts are written using manufacturer-specified application program interface (API) commands to communicate and control the amplitude and frequency output. These control signals are interfaced via the GUI as seen in Fig. 3(d).

For demonstration, a microfluidic pump (Cellix, ExiGo microfluidic syringe pump) is connected to the set-up via USB serial (Fig. 1) and controlled using select API commands. The syringe pump is triggered to generate a droplet, and the droplet volume is controlled by the flow rate and duration. This is used to create droplets of different sizes, which are then dispensed onto the SAW device surface (Supporting Movie 1). It is worth highlighting that the commercial microfluidic pump used (Cellix ExiGo) is extremely over specification for this project with nanofluidic capabilities and many unused API functions. This would be better replaced with a syringe pump built specifically for these application requirements capable of microliter droplet domain dispensing and further integration with the Raspberry Pi. In future work, we will implement an open-source pump as described in [39], using a commercial syringe pump (Cellix ExiGo) for benchmarking and comparison. It is possible to adjust this pump design to provide virtually any fluidic resolution needed via coupling the 200 step/revolution motor with an adequately sized syringe.

For instance, a Hamilton 50 μL syringe with a 60 mm stroke length would allow for the change from the mL/mm to the μL/mm scale, as each millimeter movement from the stepper motor would push 0.8 μL from the syringe. This would become the target resolution, making it capable to deliver the 1–20 μL droplets needed for reagent dispensing. Laboratory equipment such as signal generators and amplifiers helped to prove the concept in this study. In forthcoming applications, the costs and size of the set-up can be reduced by integrating chip-scale components. Both the detection and the actuation capabilities can be implemented using off-the-shelf chip-level components. For instance, using a direct digital synthesis (DDS) module as a signal generator, such as the AD9851 module (that can be bought for £10) and that operates from 0 to 70 MHz, which is a suitable range for our application. Alternatively, oscillators can be designed as resonators using well-known typologies such as Colpitts or Clapp oscillators. An integrated RFC1G21H4-24-S gallium nitride (GaN) amplifier (with a cost of $114) operated with the ADCB-20-82+ bidirectional coupler (cost £7.95) can be coupled together for device adjustment, further integration, and to optimize transfer of power. This model is rated with 2 W, which would be enough to achieve pumping. For heating, where more power is needed, we would investigate higher power GaN amplifiers. For instance, the 10-W amplifier HMC1099PM5E from Analog Devices (125€ cost inc., Norwood, MA, USA, VAT). Its compact IC form makes it ideal for integration purposes. Also, low-cost reflectometers can be implemented using RF gain/phase detectors such as AD8302 to measure the spectrum of the device.

B. Software

The GUI is implemented using Python programming language, also making use of touchscreen functionalities for more interactive user control. Via the GUI, the Raspberry Pi interfaces signal generators, RF amplifiers, microfluidic pumps, thermal imaging, and visible light cameras. Both droplet tracking and fluorescence measurements are performed using the same Raspberry Pi standard digital camera.

As a starting point, SAW operations are implemented to control droplet position, mixing, and heating. An open-source OpenCV library [42] is used for object tracking. The algorithm contains functions aimed at real-time image analysis and manipulation, with simultaneous image detection

and tracking. OpenCV library offers eight options for object tracking algorithms. Among these options, the Kernelized Correlation Filter (KCF) [43] appears to be the best all-round tracker, offering a good compromise between accuracy and speed. A proportional–integral–differential (PID) controller is then implemented using the KCF tracking in combination with Python off-the-shelf libraries. The PID controller uses the position/velocity calculated from the Raspberry Pi camera as the input control value. In the Supporting Movie 1, we have shown a side view of the selected droplet (marked with a blue bounding box) and the target position (marked with the green dot). The distance between the droplet and the target position along both the *x*- and *y*-directions are defined as the distance errors. In this study, the control system operates with a maximum of 30 fps. The precision of the PID controller is theoretically determined by the frame rate. This can have moderate fluctuations due to the computational limitations whilst running the video input stream, object tracking, PID controllers, and the GUI simultaneously, causing a varied sample rate for the input of the PID controller. We have, however, demonstrated that the current sampling rate is adequate to perform all the microfluidic functions needed to implement diagnostics with SAW. The real-time capability of the KCF tracking is limited by the Raspberry Pi platform and the Python programming to a frame rate to between 20 and 30 fps (the KCF can otherwise run at hundreds of frames per second). As the platform Raspberry Pi is periodically updated on hardware level, the concept presented here will hold its validity for future hardware upgrades.

A thermal camera is also used and allows for temperature control in a similar manner to droplet movement. The thermal camera output relays values from the droplet to another PID controller which is able to adjust the power until a target is met and maintained. Both cameras and mounted 3-D printed components are positioned above the SAW device (Fig. 1).

For fluorescence detection, a digital filter is created using Hue Saturation Value (HSV) color model. The functions of both physical optical filters and digital filters are to allow specific wavelengths of light to pass through. The digital filter uses the HSV color model to create a black-and-white mask that is then combined with the original image. The white part of the mask is where the original image is shown, and black stays its own color. To decide what will pass through to create the white section, the three variables Hue, Saturation, and Value are used. Hue is the color wheel consisting of the primary (red, blue, and yellow) and secondary colors (orange, green, and violet) in another wheel. This is a single value to represent any color from the visible spectrum. Saturation is the intensity of that color starting from no intensity of white. Value refers to the brightness of the color. Using a combination of these values, upper and lower boundaries are then set-up to create a mask. Once masked, the image is then converted to grayscale to record the brightness value. A similar grayscale technique has been used in a PCR setup using a smartphone camera [44]. Hence, using this concept in Python, it is possible to mask out every other color other than the selected range. This is highly advantageous as it allows the optical detection via conventional Raspberry Pi without the need of physical optical filters or any other advanced optical techniques, thus reducing the complexity and cost of the optical setup without jeopardizing the fluorescent detection. The upper and lower bounds are set so that only the selected color is allowed to pass through. We keep the camera parameters, such as the gains and white balance the same in every test in an effort to keep consistency. The parameters described can be effectively tuned to mask the desired wavelength and bandwidth. These bounds allow the filter to be tuned to match the fluorescence output of any dye chosen. Saturation is the measurement of white in the color. The masked image is then converted to grayscale and the brightness is recorded.

The setup presented here can be used in other applications involving SAW. The API protocols could be further developed to produce commands to enable the control GUI to set the frequency of a SAW device, connect with a camera to track a droplet, or set a target temperature among others. It is then possible to combine all related hardware into a new Python library for acoustic wave control.

C. PID Control Design for Liquid Actuation and Temperature Control

The droplet control system is designed to fulfill microfluidic protocols for DNA amplification, including droplet transport, liquid dispensing, and temperature control. For example, in DNA amplification applications, a droplet is positioned on a desired location for sample treatment, which requires such microfluidic functions. Due to variations in micro/nanofabrication process, SAW power, frequency, surface of the device, and its treatment all influence the transportation performance of a droplet, which is also varied by the sample's density and viscosity. Therefore, it is important to dynamically adjust the control parameters of these variables while maintaining the desired outcome for position control of the droplet.

The block diagram of the designed closed-loop system is shown in Fig. 4. A standard Raspberry Pi camera is used to produce a live image feed of the droplet on the surface with a top view. The KCF tracker works first by the assignment of a bounding box that the user sets around the object, which is initially placed approximately in the middle range for tracking speed and accuracy. The tracker takes a point from the box and calculates the motion by analyzing the changes between frames. Once the new point is determined, the box is recreated in the new coordinates. Once the user has selected the droplet position, the droplet will move to the target destination. The coordinates of the box center are then calculated and recorded. Once the droplet has been moved, the coordinates are recorded again, and the velocity is calculated based on the time between positions and the number of pixels in which the droplet is traveled (see Supporting Movie 2).

The controller updates (either increase, maintain, or decrease) the power outputs of the RF input signal on the forward line to maintain the target velocity and to relocate the droplet's new position, hence, minimizing
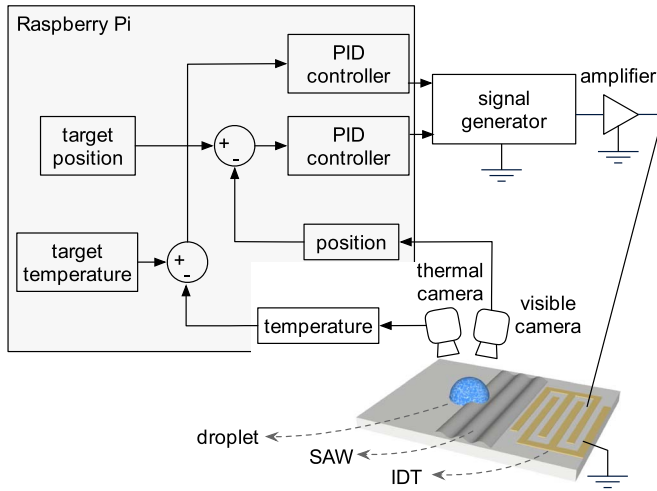
Fig. 4.   Raspberry Pi singular SAW feedback loops and module connected for droplet position and temperature control.

the distance error. The loop process operates in real-time and is terminated when the distance errors in both x- and y-directions become zero when the droplet has reached the target position. If the droplet is overshooting to another side, then the RF power will be applied to the opposite IDTs (see Supporting Movie 3), so that the droplet can be driven back to the targeted position. Using this method, we can easily control the lateral position of the droplet (Fig. 1), which has both the sample control method and separate PID controllers with nearly identical parameters in the embedded system running in parallel. A standard PID controller [45] is set to maintain a target velocity.

The PID controller used for both droplet position and temperature is expressed using the following equations:

$$e(t) = \text{SP} - \text{PV}. \qquad (1)$$

An error $e(t)$ is produced by (1) and used as the PID controller input. SP is the set point which is the target value of temperature or velocity and position. The process variable PV is the current value acquired by the thermal and visible cameras

$$u(t) = K_p e(t) + K_i \int e(t)dt + K_d \frac{de(t)}{dt}. \qquad (2)$$

The proportion gain K_p is used for a fast response getting close to the set point. The integral gain $K_i \int e(t)dt$ is used to reduce the steady-state error created by the proportional gain. The derivative gain $K_d(de(t)/dt)$ is also used to reduce overshooting and increase stability around the target value.

The position PID controller is implemented using the Python library "simple-pid" [46]. To use this module, the input parameter is set as velocity, and the target is chosen as well as output upper and lower limits, which help to protect the SAW device. Then the proportional, integral, and differential gain values are set to reduce the time that it takes for the droplet to overcome the friction force on the surface and start moving while reducing over-shooting oscillation around the set target velocity. The gain values depend also on the volume and contact angle of the droplet to the surface, which

is dependent on the surface treatment. The platform allows for further self-tuning PID values by using machine learning Python libraries, which will be considered in future work.

The temperature PID controller is also implemented with "simple-pid" library. Temperature control is established by implementing a PID controller with infrared camera readings as input process variable and SAW device supply as output. The thermal camera, calibrated with a separate infrared camera setup, is used for monitoring temperatures. The thermal camera is connected via the GPIO pins and is communicated using serial peripheral interface (SPI). The position of the droplet is selected and the temperature values from the camera are used to continuously monitor the sample at 8 Hz. Once the user starts the assay, the temperature is fed into the PID which sets the power sent to the SAW device to aim for the set point desired temperature in a similar way as the position control.

An inherent property of PZTs is the dependency of their resonant frequency to their temperature due to material properties. The dependency is measured with the temperature coefficients of frequency (TCF). Due to the thermal effect [47], the frequency is shifted as the temperature of the SAW device changes. We use the thermal imaging to feedback the temperature value of the IDT surface alongside the droplet and use the TCF equation described in [47] to calculate and compensate the new frequency signal applied, matched with the new resonant frequency. Every time the droplet temperature is measured, the surface is recorded and used to calculate the adjusted frequency

$$F_{\text{new}} = F_0 + \Delta F. \qquad (3)$$

where F_0 is the device frequency measured at room temperature before starting the assay, and ΔF is the change in frequency

$$\Delta F = \text{TCF} \cdot T \cdot \Delta F_0 \qquad (4)$$

where TCF is the temperature coefficient of the frequency for the device, and ΔT is the change of temperature.

D. Fluorescence Detection

In PCR or LAMP assays, the targeted DNA strands are typically multiplied while producing chemiluminescence signals. The detection of a positive sample is replicated by measuring the luminescence of fluorescent dyes. In this study, a liquid solution of quinine is employed for fluorescence measurement testing. Quinine contains phosphorous, a material that emits light when exposed to 300–400 nm wavelengths of the electromagnetic spectrum. When the ultraviolet (UV) light is absorbed in the quinine, the substance changes into blue color. A UV LED was used for this purpose (i.e., UV5TZ Series UV LED Array, 385 nm 20 mW, 15°, 2-Pin Through Hole from manufacturer Bivar).

Using computer vision to process the visible light camera, the brightness of the sample is monitored and displayed on the GUI as seen in Fig. 5. The excitation source for fluorescence is a conventional 5-mm diameter LED, which meets the specific wavelength emission required for the dye chosen. For example, the Synergy Brands Inc., NY, New York, USA, (SYBR) green
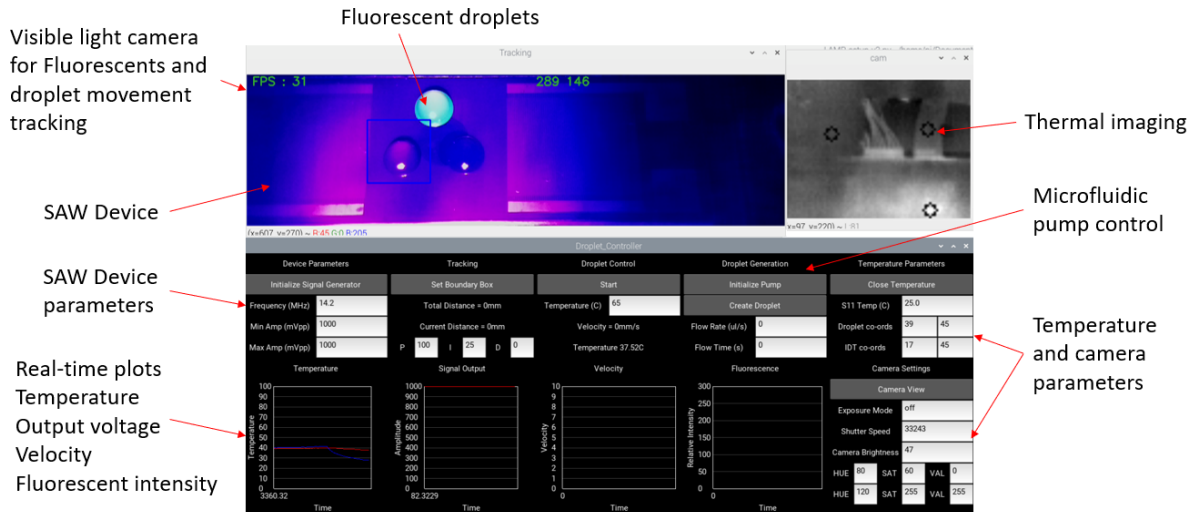
Fig. 5. Print screen of the GUI with fluorescence measurements.

is a commonly used fluorescent dye that binds to the target DNA [5]. The dye requires an excitation light source with a wavelength of 497 nm, causing the sample to emit light with a wavelength centered at 520 nm [48]. Then, a blue LED that has the dominant wavelength of 480 nm that is close to the most efficient excitation wavelength (4 V Blue LED 5 mm Through Hole, Cree C503B-BCN-CV0Z0461) can be used. The visible light camera monitors the light emitted from the same known as the excitation wavelength.

E. SAW Device Fabrication and Surface Treatment

The electronic setup is designed to be used with any SAW device. In the results presented here, we make use of thin-film-based SAW devices. Thin-film SAW devices, that is, those based on ZnO/Al and AlN/Si substrates, do not exhibit the problems of bulk substrates such as in-plane anisotropic piezoelectric properties, inflexibility, brittleness, and difficulty to control/realize different wave modes [49]. Thin-film SAW presents additional advantages such as hierarchical nanotexturing on a variety of substrates [50]. Ultralow cost can be achieved with scaling-up volume production industrially, although to achieve thicker film it will take longer deposition times and potential film stress issues. Previous SAW-based DNA amplification works [14], [15] used crystal-based piezoelectric devices (such as $LiNbO_3$), which are brittle and costly. Thin-film SAW has also recently been demonstrated as efficient microheaters [51]. In this study, we used ZnO/Al sheet SAW devices [50], [52].

Piezoelectric ZnO thin films were deposited onto the Al plate (1.6-mm thick) using direct-current (dc) magnetron sputter coating techniques. A zinc target with 99.99% purity was used for the deposition, with an Ar/O_2 flow ratio of 10/15 sccm. The dc power was 400 W, and the gas pressure was 4×10^{-4} mbar.

The sample holder was rotated during the deposition to achieve uniform films with a rate of 5.6 nm/min. The thickness of ZnO thin films was ~10 μm. This relatively thicker film

is used to have a good piezoelectric effect to generate strong acoustic waves for microfluidic operations.

The interdigital transducers (IDTs) are composed of sputter-coated Al with a thickness of 200 nm prepared through a conventional photolithography and lift-off process. The IDTs have a wavelength of 200 μm, with 50 pairs of fingers and an aperture of 5 mm. The Rayleigh wave frequency of the SAW devices is measured as ~14.3 MHz. This frequency is chosen so that there is no significant damping effect of waves when compared to higher frequency devices. The surface of the device is treated using biocompatible fluoropolymer coating CYTOP solution (L-809A from AGC Chemicals, Exton, PA, USA) for hydrophobic coating. The solution is applied onto the top surface of the SAW device via a dip-coating method and heated to 180 °C for 10 min. A vector network analyzer (Keysight Fieldfox portable vector network analyzer, N9913A 4 GHz) is used to measure the reflection spectrum S_{11} of the devices (see supporting information Fig. 1).

III. RESULTS AND DISCUSSION

A. Acoustofluidics for Integral and Remote Droplet Position Control

We demonstrate the remote-control functions of generation, pumping, moving, and mixing of single and multiple droplets, applied in a sequential order. We also test the performance of the setup in inclined angles, and we test transport droplets in multiple directions to any location on a surface using multiple PID controllers in the lateral plane. During these movements, a target speed is set.

Fig. 6(a) shows one example of the targeted velocity, measured velocity, and the power sent to the SAW device. The PID controller sets the output voltage generated from the signal generator which is amplified and transmitted. After the initial transient, the velocity oscillates around the target velocity with moderate power oscillation. The PID helps to keep momentum in the droplet as it travels across the device, preventing the significant changes of velocity in the event of a non-uniformly treated surface. In this typical example, the time takes 5 s, and
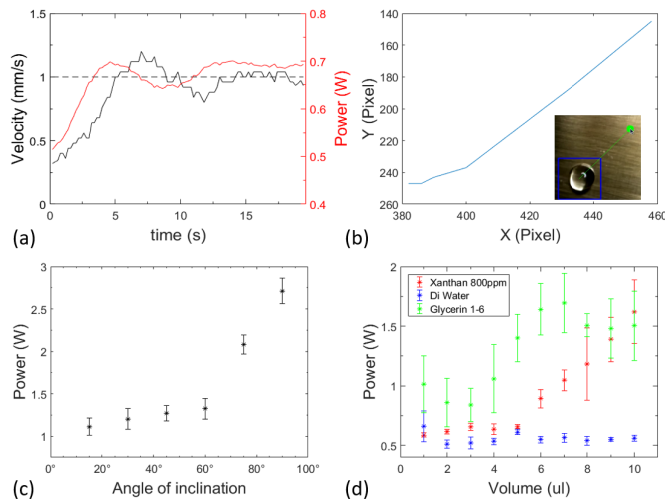
Fig. 6. (a) 10-μL droplet movement. (b) Droplet movement using multiple IDTs. (c) Droplet movement on increased substrate inclination angle. (d) Effect of viscosity on droplet movement.

Fig. 7. Droplet mixing of microparticles. (a) No movement. (b) 0.5 s into movement. (c) Droplet merging. (d) Droplet mixing.

the overshoot is 20%. Once settled after 13 s, the steady-state error of movement is ±0.2 mm/s. The droplet will usually stop within 0.5 mm of the destination.

Fig. 6(b) represents an example of droplet movement in the x- and y-positions over 5 s. Separate signal sources and PID controllers are used with multiple IDTs allowing the droplet to be propelled diagonally. This was used and recorded with a potential touchscreen in the future. In supporting videos (Supporting Movies 4 and 5), when the user clicks (or places the finger on the screen) a trajectory green line appears between the droplet and the curser location. As the droplet moves, both x- and y-axis values are represented as the example shown in Fig. 6(a). Note that in [14] and [15] single assays are performed using only one IDT as the fluidic dispensing protocol is set to be sequential. The four electrodes controlled by the setup here could be rearranged in a different configuration (e.g., in parallel lines instead of in a cross) to have four assays running in parallel. This might be the easiest way to multiplex the system's operation. Fig. 6(c) shows the obtained powers required for transportation of droplets along inclined surfaces with different inclination angles from 15° to 90°. It should be noted that the hierarchical nanotexturing fabrication (as in [50]) exploits a unique combination of shear hydrophobicity and tensile hydrophilicity. The obtained nanostructured surfaces are, at the same time, both slippery (low in-plane pinning) and sticky (high normal-to-plane liquid adhesion), which allow droplets to sit in inclined (or even vertical) angles. The aim is to demonstrate in-field operation, where there might not be flat surfaces to accommodate the setup, and also demonstrate that the controller adapts its PID values in uneven surfaces. The set distance is 10 mm, the target velocity is set as 1 mm/s, and the volume of the droplet is 2 μL.

Finally, we have further investigated the ability to control liquids with various rheological behaviors, which could be explored for further biological applications such as separating plasma from whole blood [53] or cell sorting [54]. Diff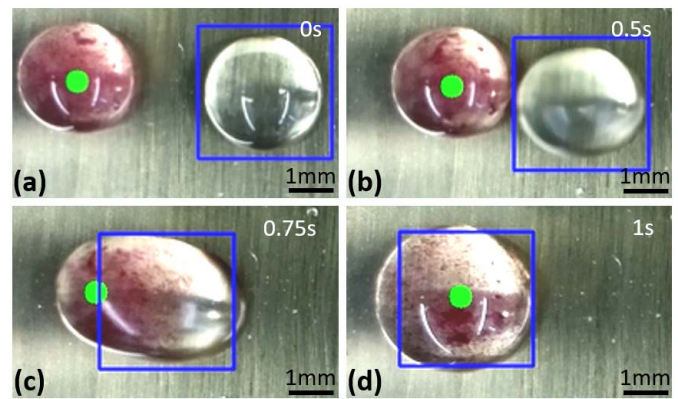erent types of Newtonian and non-Newtonian fluids are used in the experiments. Most experiments are performed using deionized water (DI) with viscosity and density of 1.0016 mPa.s and 995.0 kg/m^3, respectively. We also tested 17.388 (wt%) aqueous glycerol solution to investigate the effect of higher viscosity for Newtonian fluids. The kinematic viscosity and density of this solution are 1.5631 mPa.s and 1039.8 kg/m^3, respectively. To simulate the non-Newtonian behavior of liquids such as blood, droplets of Xanthan solution (molecular weight, Mw $\sim 10^6$ g.mol^{-1}, Sigma Aldrich) [55] with concentration of 800 (ppm w/w) and density 995.4 kg/m^3 are used in the experiments. The power law ($\mu = 0.076 \dot{\gamma}^{0.51}$, where $\dot{\gamma}$ is the shear rate in the flow) is used to calculate the viscosity of the solution.

Fig. 6(d) shows the average powers required for different types of liquids to be transported at a designed velocity of 1 mm/s. The power values are measured at the connection to the SAW device from the amplifier output, where we report the power measured at the output of the amplifier. The data from the pure water droplet is used as a reference. The data for the Newtonian fluids with higher viscosities show that by increasing the liquid viscosity, the minimum power to start the droplet motion is increased. Furthermore, higher powers are needed to keep the droplet moving with the consistent velocity. Another interesting result is the dependency of the minimum power to the droplet size. Since Xanthan solution is a shear-thinning liquid, due to the generation of an internal streaming field within the droplet (and increasing the shear rate), the viscosity of the liquid is decreased. Thus, less energy is dissipated by liquid viscosity and the droplet can be transported using a lower power on the surface. The internal streaming velocity field is more intense for smaller droplets and thus lower powers are needed to move the droplet. Due to the fabrication process and the hydrophobic surface treatments, SAW devices have variations in frequency and peaks. These two factors (device fabrication and surface treatment) influence the efficiency of the device. The differences in device efficiencies are observed even in the same batch. This is a common issue in micro/nano-fabricated products, and in commercial applications this is resolved with the inclusion of a calibration step.

We further demonstrate the mixing functions for remote control of biological or blood dilution washing. One of the examples for droplet mixing is shown in Fig. 7. One droplet
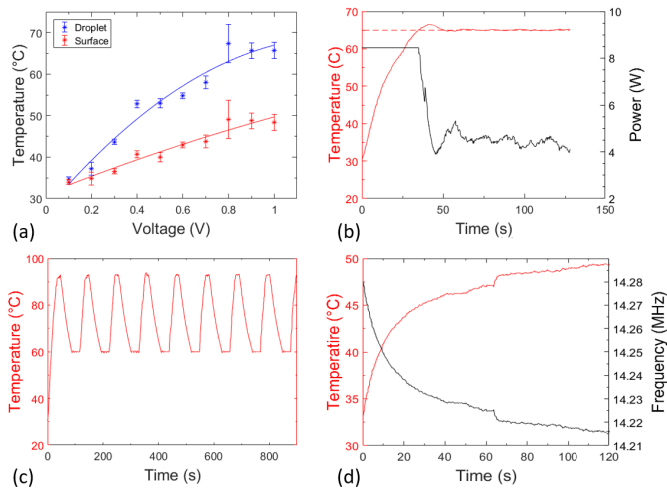
Fig. 8. (a) Temperature recordings for droplet and surface using a constant input voltage (peak-to-peak). (b) Example of droplet temperature control (simulated LAMP thermal process). (c) Example of droplet temperature control (simulated PCR thermal cycling). (d) Example control of frequency over time.
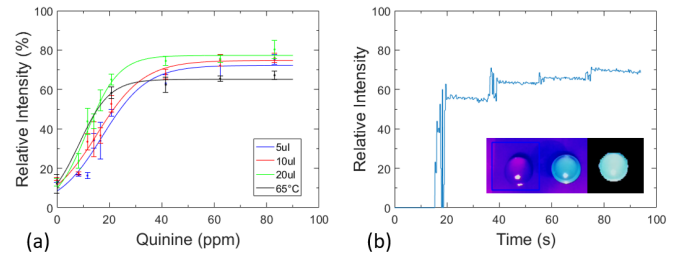

Fig. 9. (a) Fluorescence concentration and relative intensity, measured at room temperature and 10 μL at 65 °C. (b) Example mixing of fluorescent droplets over time.

with red polystyrene is transported to move and mix with another one of pure DI water. To mix fluids thoroughly, the distribution of the particles on the droplet is monitored using the digital camera. The duration of the mixing is set arbitrarily to the point where the microparticles appear homogenously distributed in the droplet. This mixing protocol can be adjusted and optimized based on the application at hand. The droplet of DI water is chosen as the tracking boundary and the droplet with red polystyrene as the destination. The DI water is pumped to the droplet with red polystyrene and two droplets are mixed into one larger droplet. With further IDT actuators combined with additional processing capabilities, it is possible to scale the system to track several droplets to transport or mix/dilute. In order to control and move multiple droplets independently, the SAW devices could be manufactured with an increased number of IDTs on the 2-D plane creating a matrix in which several droplets can be actuated at the same time.

B. Temperature Control

This section demonstrates thermal cycling for PCR and LAMP reactions. For this, we use a sessile droplet of DI water with volumes of 10 μL. These droplets are dispensed onto the surface where their locations are found, as well as the target temperatures and control parameters are set.

Fig. 8(a) shows the differences in temperatures between the IDT surface and the droplet in front. The peak-to-peak voltage in the *x*-axis refers to the input at the amplifier. This shows the energy transfer into the droplet and enabling the adjustment of the IDT frequency to maintain efficiency as shown in Fig. 8(d). This opens up the possibility to control droplet temperature without thermal camera need, using the surface temperature or even the frequency shift and the TCF equation to calculate the temperature at the droplet.

In LAMP reactions, the sample is typically heated to 65 °C for an interval of 20–30 min. Fig. 8(b) shows an example of reaching and maintaining 65 °C, demonstrating the control

function of droplet heating using the PID controller described in Section II-B. The values used are a proportional gain of 100 and an integral gain of 25. The differential gain in this case is set to 0, making this currently a proportional integral (PI) controller. The droplet is heated to a temperature to 65 °C for 2 min. The time taken to reach the target temperature from 30 °C takes 35–40 s. The settling time takes a further 10–20 s with an overshoot of 2%. Once at temperature, the algorithm is able to stabilize and maintain the temperature with an accuracy ±0.3 °C. The accuracy of the temperature is similar to that of a certified thermal cycler. LAMP reactions operate most efficiently between 60 °C and 70 °C, making this platform easily suitable for DNA amplification assays.

Fig. 8(c) is an example of PCR temperature cycling (60 °C–90 °C). In a PCR reaction, this routine lasts 40 cycles. The precision of this temperature control allows for PCR to function and is capable of holding set points for 20–30 s. The set point can be automatically timed and changed as part of the Python program feeding into the PID controller.

For both Fig. 8(b) and (c), the IDT is driven using the Rayleigh resonant frequency, which for the device employed (standard electrode design with $\lambda = 200\ \mu$m), this is in the order of 14 MHz. This resonant wave mode can be employed for both heating and pumping; hence, a fine balance needs to be established between heating performance and droplet integrity. During thermal cycling in Fig. 8(c), we place the droplet in a single spot that has not been hydrophobically treated, which helps with anchoring the droplet. Moreover, to avoid droplet evaporation, we coat this with mineral oil as similar to [14]. In the future, we might investigate whether heating performance can be improved by using two IDTs. In principle, this would allow to perform thermal cycling without an anchoring spot. However, two PID controllers would need to be actuated in parallel while balancing the microfabrication tolerances between the electrodes, which influence the resonant peak region and depth.

C. Fluorescent Relative Intensity

Fluorescent measurements are investigated using our system using various concentrations and droplet sizes. We measure the input grayscale brightness (relative intensity) using the Raspberry Pi visible light camera based on our developed platform. By controlling the concentration of quinine, we show that the droplet fluorescence signals under the 385-nm UV light can be monitored.

Fig. 9(a) shows the fluorescence signals of droplets with different volumes, which show varied fluorescent levels. Adjusting the volume of the droplet affects the recorded brightness obtained by the camera. This variation is a maximum of 15%, because of the differences in the areas to absorb UV light and emit blue light. As the concentration of quinine is increased, the measured fluorescence signal is increased. As the solution is further diluted with DI water below 20 ppm, the fluorescence intensity begins to rapidly decrease to 8 ppm (e.g., 10% of the initial quinine concentration). At this point, with the current camera and settings, it can no longer distinguish the droplet from the pure DI water.

Fig. 9(b) shows the measurement results for the real time mixing. Starting with 5 μL DI water, the digital filter detects no value. When a 5 μL of quinine solution is mixed with the water driven by the SAW from one side, the brightness increases. The growth of intensity is more significant for the first mixing of solution, and further introduction of solutions results in stagnated increase of intensity (because of the increase of total volume of the droplet). There are noise signals introduced as the droplets merge and mix before settling. Quinine represents the DNA amplification in the testing of this system. Increasing the quantity in the solution also begins to reach a point where further increasing the concentration does not yield further fluorescent intensity.

IV. CONCLUSION

In this work, we have presented Acousto-Pi, a versatile and adaptable opto-acoustofluidic platform with embedded open-source electronics for biological assay applications. The platform can be used to interface and control any SAW device. Using thin-film SAW devices, we simulate a biological reaction for DNA amplification by showing all the specific steps that an opto-acoustofluidic system needs to achieve. We have demonstrated the ability to control and monitor the motion of droplets of several sizes, allowing for transportation and mixing of reagents. Utilizing a similar feedback control loop, the temperature of the samples can be set to a range of target values. These temperatures can be maintained with multiple different droplet sizes. Apart from the ability to manipulate droplets, digital optical fluorescent measurements are also implemented, resulting in a combined acoustofluidic and optical sensing platform. The setup is an adaptable system that can be adjusted to be used on different assays, including variations in target temperature, volume, or type of reagents and samples used. The platform also compensates for SAW device fabrication and surface treatments, as well as temperature-induced resonant frequency shifts. Using open-source technology, additional functions can be included, allowing for a large amount of modularity without a large increase in complexity. The platform provides embedded computation which can be used for data storage, cloud transmission, and further applications using machine-learning algorithms.

ACKNOWLEDGMENT

REFERENCES

[1] Y. Hassan and L. T. L. Than, "Loop-mediated isothermal amplification (LAMP): Comparative advances over conventional PCR and other molecular techniques," *Annu. Res. Rev. Biol.*, vol. 35, no. 8, pp. 33–44, Aug. 2020.

[2] A. Raghunathan, H. R. Ferguson, C. J. Bornarth, W. Song, M. Driscoll, and R. S. Lasken, "Genomic DNA amplification from a single bacterium," *Appl. Environ. Microbiol.*, vol. 71, no. 6, pp. 3342–3347, Jun. 2005.

[3] A. Barakat *et al.*, "Diagnostic testing for SARS-CoV-2," World Health Org., Geneva, Switzerland, Interim Rep., 2020, pp. 1–20.

[4] B. Schermer *et al.*, "Rapid SARS-CoV-2 testing in primary material based on a novel multiplex RT-LAMP assay," *PLoS ONE*, vol. 15, no. 11, Nov. 2020, Art. no. e0238612.

[5] A. Evrard, N. Boulle, and G. S. Lutfalla, *Real-Time PCR*. Berlin, Germany: Springer, 2010.

[6] T. J. Moehling, G. Choi, L. C. Dugan, M. Salit, and R. J. Meagher, "LAMP diagnostics at the point-of-care: Emerging trends and perspectives for the developer community," *Expert Rev. Mol. Diag.*, vol. 21, no. 1, pp. 43–61, Jan. 2021.

[7] T. Notomi *et al.*, "Loop-mediated isothermal amplification of DNA," *Nucleic Acids Res.*, vol. 28, no. 12, p. 63, Jun. 2000.

[8] M. C. Giuffrida and G. Spoto, "Integration of isothermal amplification methods in microfluidic devices: Recent advances," *Biosens. Bioelectron.*, vol. 90, pp. 174–186, Apr. 2017.

[9] Y. Q. Fu *et al.*, "Recent developments on ZnO films for acoustic wave based bio-sensing and microfluidic applications: A review," *Sens. Actuators B, Chem.*, vol. 143, no. 2, pp. 606–619, Jan. 2010.

[10] J. Zhang *et al.*, "Surface acoustic waves enable rotational manipulation of caenorhabditis elegans," *Lab Chip*, vol. 19, no. 6, pp. 984–992, Mar. 2019.

[11] K. Wang *et al.*, "Sorting of tumour cells in a microfluidic device by multi-stage surface acoustic waves," *Sens. Actuators B, Chem.*, vol. 258, pp. 1174–1183, Apr. 2018.

[12] M. Rotter, A. V. Kalameitsev, A. O. Govorov, W. Ruile, and A. Wixforth, "Charge conveyance and nonlinear acoustoelectric phenomena for intense surface acoustic waves on a semiconductor quantum well," *Phys. Rev. Lett.*, vol. 82, no. 10, pp. 2171–2174, Mar. 1999.

[13] S. Alzuaga *et al.*, "A large scale X-Y positioning and localisation system of liquid droplet using SAW on LiNbO/sub3," in *Proc. IEEE Symp. Ultrason.*, Oct. 2004, pp. 1790–1793.

[14] J. Reboud *et al.*, "Shaping acoustic fields as a toolset for microfluidic manipulations in diagnostic technologies," *Proc. Nat. Acad. Sci. USA*, vol. 109, no. 38, pp. 15162–15167, 2012.

[15] G. Xu, R. N. Gunson, J. M. Cooper, and J. Reboud, "Rapid ultrasonic isothermal amplification of DNA with multiplexed melting analysis—Applications in the clinical diagnosis of sexually transmitted diseases," *Chem. Commun.*, vol. 51, no. 13, pp. 2589–2592, 2015.

[16] G. Papadakis *et al.*, "3D-printed point-of-care platform for genetic testing of infectious diseases directly in human samples using acoustic sensors and a smartphone," *ACS Sens.*, vol. 4, no. 5, pp. 1329–1336, May 2019.

[17] K. Tsougeni *et al.*, "Lab-on-chip platform and protocol for rapid foodborne pathogen detection comprising on-chip cell capture, lysis, DNA amplification and surface-acoustic-wave detection," *Sens. Actuators B, Chem.*, vol. 320, Oct. 2020, Art. no. 128345.

[18] Z. Ramshani *et al.*, "Extracellular vesicle microRNA quantification from plasma using an integrated microfluidic device," *Commun. Biol.*, vol. 2, no. 1, pp. 1–9, 2019.

[19] H. Zhang, Y. Xu, Z. Fohlerova, H. Chang, C. Iliescu, and P. Neuzil, "LAMP-on-a-chip: Revising microfluidic platforms for loop-mediated DNA amplification," *TrAC Trends Anal. Chem.*, vol. 113, pp. 44–53, Apr. 2019.

[20] H. Bachman *et al.*, "Acoustofluidic devices controlled by cell phones," *Lab Chip*, vol. 18, no. 3, pp. 433–441, 2018.

[21] L. Zhang, Z. Tian, H. Bachman, P. Zhang, and T. J. Huang, "A cell-phone-based acoustofluidic platform for quantitative point-of-care testing," *ACS Nano*, vol. 14, no. 3, pp. 3159–3169, Mar. 2020.

[22] J. P. Lata, F. Guo, J. Guo, P. Huang, J. Yang, and T. J. Huang, "Surface acoustic waves grant superior spatial control of cells embedded in hydrogel fibers," *Adv. Mater.*, vol. 28, no. 39, pp. 8632–8638, Oct. 2016.

[23] M. Yousefi, O. Pourmehran, M. Gorji-Bandpy, K. Inthavong, L. Yeo, and J. Tu, "CFD simulation of aerosol delivery to a human lung via surface acoustic wave nebulization," *Biomech. Model. Mechanobiol.*, vol. 16, no. 6, pp. 2035–2050, Dec. 2017.

[24] K. M. Ang, L. Y. Yeo, J. R. Friend, Y. M. Hung, and M. K. Tan, "Nozzleless spray cooling using surface acoustic waves," *J. Aerosol Sci.*, vol. 79, pp. 48–60, Jan. 2015.

[25] Y. Q. Fu *et al.*, "Advances in piezoelectric thin films for acoustic biosensors, acoustofluidics and lab-on-chip applications," *Prog. Mater. Sci.*, vol. 89, pp. 31–91, Aug. 2017.

[26] C. Song *et al.*, "Opto-acousto-fluidic microscopy for three-dimensional label-free detection of droplets and cells in microchannels," *Lab Chip*, vol. 18, no. 9, pp. 1292–1297, 2018.

[27] B. Hu *et al.*, "An opto-acousto-fluidic microscopic system with a high spatiotemporal resolution for microfluidic applications," *Opt. Exp.*, vol. 27, no. 2, pp. 1425–1432, Jan. 2019.

[28] W. Watanabe, R. Maruyama, H. Arimoto, and Y. Tamada, "Low-cost multi-modal microscope using Raspberry Pi," *Optik*, vol. 212, Jun. 2020, Art. no. 164713.

[29] A. M. Chagas, L. L. Prieto-Godino, A. B. Arrenberg, and T. Baden, "The ε100 lab: A 3D-printable open-source platform for fluorescence microscopy, optogenetics, and accurate temperature control during behaviour of zebrafish, Drosophila, and Caenorhabditis elegans," *PLOS Biol.*, vol. 15, no. 7, Jul. 2017, Art. no. e2002702.

[30] T. Aidukas, R. Eckert, A. R. Harvey, L. Waller, and P. C. Konda, "Low-cost, sub-micron resolution, wide-field computational microscopy using opensource hardware," *Sci. Rep.*, vol. 9, no. 1, pp. 1–12, May 2019.

[31] Y. Temiz, "The lego microscope: A valuable lab tool began as a diy project–[hands on]," *IEEE Spectr.*, vol. 57, no. 5, pp. 16–18, May 2020.

[32] M. Liu, Z. Tang, H. Monshat, Y. Zhao, and M. Lu, "Portable instrument for paper-based isothermal nucleic acid amplification tests," in *Proc. Conf. Lasers Electro-Opt.*, vol. 1, 2020, pp. 1–3.

[33] A. Marzo, T. Corkett, and B. W. Drinkwater, "Ultraino: An open phased-array system for narrowband airborne ultrasound transmission," *IEEE Trans. Ultrason., Ferroelectr., Freq. Control*, vol. 65, no. 1, pp. 102–111, Jan. 2018.

[34] H. Bachman *et al.*, "Open source acoustofluidics," *Lab Chip*, vol. 19, no. 14, pp. 2404–2414, 2019.

[35] A. Huang *et al.*, "Practical microcircuits for handheld acoustofluidics," *Lab Chip*, vol. 21, no. 7, pp. 1352–1363, 2021.

[36] J. Matouš, A. Kollaršík, M. Gurtner, T. Michálek, and Z. Hurák, "Optimization-based feedback manipulation through an array of ultrasonic transducers," *IFAC-PapersOnLine*, vol. 52, no. 15, pp. 483–488, 2019.

[37] I. Nuñez *et al.*, "Low cost and open source multi-fluorescence imaging system for teaching and research in biology and bioengineering," *PLoS ONE*, vol. 12, no. 11, Nov. 2017, Art. no. e0187163.

[38] J. M. Pearce, "Laboratory equipment: Cut costs with open-source hardware," *Nature*, vol. 505, no. 7485, p. 618, 29-Jan-2014.

[39] B. Wijnen, E. J. Hunt, G. C. Anzalone, and J. M. Pearce, "Open-source syringe pump library," *PLoS ONE*, vol. 9, no. 9, pp. 1–8, 2014.

[40] *What the App Does NHS COVID-19 App Support NHS.UK*. Accessed: Dec. 11, 2020. [Online]. Available: https://covid19.nhs.uk/what-the-app-does.html

[41] *MIPI Overview*. Accessed: Sep. 6, 2019. [Online]. Available: https://www.mipi.org/about-us

[42] A. Spizhevoy and A. Rybnikov, *OpenCV 3 Computer Vision*. Birmingham, U.K.: Packt, 2018.

[43] J. F. Henriques, R. Caseiro, P. Martins, and J. Batista, "High-speed tracking with kernelized correlation filters," *IEEE Trans. Pattern Anal. Mach. Intell.*, vol. 37, no. 3, pp. 583–596, Mar. 2015.

[44] J.-D. Kim, C.-Y. Park, Y.-S. Kim, and J.-S. Hwang, "Quantitative analysis of fluorescence detection using a smartphone camera for a PCR chip," *Sensors*, vol. 21, no. 11, p. 3917, Jun. 2021.

[45] A. Z. Leal, "Probably the best simple PID tuning rules in the world," *Antimicrob. Agents Chemother.*, vol. 53, no. 95, pp. 45–52, 2012.

[46] M. Lundberg. (2018). *Welcome to Simple-Pid's Documentation! Simple-Pid 0.1 Documentation*. Accessed: Nov. 5, 2019. [Online]. Available: https://simple-pid.readthedocs.io/en/latest/

[47] R. Tao *et al.*, "Bimorph material/structure designs for high sensitivity flexible surface acoustic wave temperature sensors," *Sci. Rep.*, vol. 8, no. 1, pp. 1–9, Dec. 2018.

[48] *SYBR Green I Nucleic Acid Gel Stain Useful Tips*, Molecular Probes, Invitrogen, Waltham, MA, USA, 2003, pp. 1–5.

[49] R. Tao *et al.*, "Thin film flexible/bendable acoustic wave devices: Evolution, hybridization and decoupling of multiple acoustic wave modes," *Surf. Coatings Technol.*, vol. 357, pp. 587–594, Jan. 2019.

[50] R. Tao *et al.*, "Hierarchical nanotexturing enables acoustofluidics on slippery yet sticky, flexible surfaces," *Nano Lett.*, vol. 20, no. 5, pp. 3263–3270, May 2020.

[51] Y. Wang *et al.*, "A rapid and controllable acoustothermal microheater using thin film surface acoustic waves," *Sens. Actuators A, Phys.*, vol. 318, Feb. 2021, Art. no. 112508.

[52] Y. Wang *et al.*, "Flexible/bendable acoustofluidics based on thin-film surface acoustic waves on thin aluminum sheets," *ACS Appl. Mater. Interface*, vol. 13, no. 14, pp. 16978–16986, Apr. 2021.

[53] L. Y. Yeo and J. R. Friend, "Surface acoustic wave microfluidics," *Annu. Rev. Fluid Mech.*, vol. 46, pp. 379–406, Jan. 2014.

[54] L. Y. Yeo and J. R. Friend, "Ultrafast microfluidics using surface acoustic waves," *Biomicrofluidics*, vol. 3, no. 1, Jan. 2009, Art. no. 12002.

[55] S. Varagnolo, G. Mistura, M. Pierno, and M. Sbragaglia, "Sliding droplets of xanthan solutions: A joint experimental and numerical study," *Eur. Phys. J. E*, vol. 38, no. 11, pp. 1–8, Nov. 2015.

Jethro Vernon received the M.Eng. degree (Hons.) in electrical and electronic engineering from the University of Northumbria, Newcastle upon Tyne, U.K., in 2018, where he is currently pursuing the Ph.D. degree.

He is currently working with piezo electric thin-film surface acoustic waves for biomedical applications. His experience and expertise is in the integration of electronics, sensors, and software.

Pep Canyelles-Pericas (Member, IEEE) received the B.Eng. (double degree) in electrical and electronic engineering from the Technical University of Catalonia, Barcelona, Spain, and the University of Northumbria, Newcastle upon Tyne, U.K., in 2006; the M.Sc. degree in engineering management from the University of Sunderland, Sunderland, U.K., in 2008; and the Ph.D. degree in control systems (he studied nonlinear state observers) from the University of Northumbria, in 2016.

Between 2009 and 2012, he worked as a Optoelectronics Research Engineer with the University of the Balearic Islands, Palma, Spain. After Ph.D. graduation, he engaged with the Innovate U.K. projects in the Knowledge Transfer Partnership (KTP) and the Innovation to Commercialization of University Research (ICURe) schemes. Since 2019, he has been a Researcher with the MESA+ Institute of Nanotechnology, University of Twente, Enschede, The Netherlands. His research interests are acoustofluidics, optical sensing, instrumentation, and control.

Hamdi Torun was an Associate Professor with Bogazici University, Istanbul, Turkey. He is an Associate Professor with Northumbria University, Newcastle upon Tyne, U.K. He is a Co-Founder of GlakoLens, a biomedical spinoff, in Istanbul.

Mr. Torun was a recipient of the Marie Curie Fellowship (MC-IRG Grant) in 2011, the Innovator Under 35 Award from MIT Tech Review in 2014, the Technology Award from Elginkan Foundation, Turkey, in 2016, Young Scientist Award from The Science Academy, Turkey, in 2016. His expertise is in development of integrated micro/nanosystems especially for sensing applications.

Xuewu Dai received the B.Eng. degree in communication engineering and the M.Sc. degree in computer science from Southwest University, Chongqing, China, in 1999 and 2003, respectively, and the Ph.D. degree in electrical and electronic engineering from The University of Manchester, Manchester, U.K., in 2008.

Prior to the Lecturer position with University of Northumbria, Newcastle upon Tyne, U.K., he held two Research Associate positions with the University of Oxford, Oxford, U.K., from 2011 to 2013, and University College London, London, U.K., from 2009 to 2011, respectively, to develop the wireless condition monitoring system for aero engine testing and the signal processing system of noncontact optical sensor for wastewater and environment monitoring with industrial partners. His research interests include advanced signal processing and its applications in control systems and wireless communications.

Dr. Dai was a recipient of the Early Career Research Prize by SWIG U.K.

Wai Pang Ng (Senior Member, IEEE) received the B.Eng. degree (Hons.) in communications and electronic engineering from the University of Northumbria, Newcastle upon Tyne, U.K., in 1997, and the Ph.D. degree in electronic engineering from the University of Wales, Swansea, U.K., in 2001.

He has worked as a Senior Networking Software Engineer with Intel Corporation, Santa Clara, CA, USA. He is currently the Deputy Head of Department and an Associate Professor of optical communications with the Department of Math, Physics and Electrical Engineering, Northumbria University, Newcastle upon Tyne. His research interests include radio-over-fiber, cognitive radio, high speed optical communications, adaptive digital signal processing, and distributed fiber sensing.

Richard Binns received the B.Eng. degree in electronic and information engineering and the Ph.D. degree in analog test strategies from Huddersfield University, Huddersfield, U.K., in 1993 and 1997, respectively.

He is the Head of the Department of Mathematics Physics and Electrical Engineering and an Associate Professor with Northumbria University, Newcastle upon Tyne, U.K. He moved to Northumbria University, in 2001, on an EPSRC Post-Doctoral Contract looking into Analog Synthesis tool development in collaboration with Ericson Components and Cadence Design Systems, San Jose, CA, USA. His current research work is varied from the design of electronics for visible light communications, energy management in electric vehicles, research into radiation detection mechanisms for personal dosimetry, and power control systems development.

Krishna Busawon (Senior Member, IEEE) received the B.Sc. degree in mathematics and fundamental sciences from the University of St-Etienne, Saint-Étienne, France, in 1989, the B.Eng. and M.Sc. degrees in electrical engineering, and the M.Phil. and Ph.D. degrees in control systems engineering from the University of Lyon, Lyon, France, in 1990, 1991, 1992, and 1996, respectively.

He was appointed as a Research Fellow with Simon Fraser University, Burnaby, BC, Canada, in 1997. Following this, he joined the University of Nuevo León, San Nicolás de los Garza, Mexico, as a Lecturer. In 2000, he joined Northumbria University, Newcastle upon Tyne, U.K., as a Senior Lecturer. In 2008, he became a Reader in control systems engineering and a Professor in February 2013. He is a Professor in control systems engineering with the Faculty of Engineering and Environment, Northumbria University. His research interests are in mathematical modeling, nonlinear control, nonlinear observer design, fault detection, and isolation.

Yong-Qing Fu received the Ph.D. degree from Nanyang Technological University, Singapore, in 1999.

He worked as a Research Associate with the University of Cambridge, Cambridge, U.K. He was a Lecturer with Heriot-Watt University, Edinburgh, U.K., and then a Reader with the Thin Film Centre, University of West of Scotland, Glasgow, U.K., before moving to Newcastle, U.K., in 2015. He is a Professor with the Faculty of Engineering and Environment, University of Northumbria, Newcastle upon Tyne, U.K. He has extensive experience in smart thin films/materials, biomedical microdevices, energy materials, lab-on-chip, micromechanics, MEMS, nanotechnology, sensors, and microfluidics. He has published more than 400 science citation index (SCI) journal articles and his current SCI H-index is 55.